ARTICLE

Near-Infrared Phosphorescent Polymeric Nanomicelles: Efficient Optical Probes for Tumor Imaging and Detection

Rajiv Kumar,[†] Tymish Y. Ohulchanskyy,[†] Indrajit Roy,[†] Sandesh K. Gupta,[†] Carsten Borek,[‡] Mark E. Thompson,[‡] and Paras N. Prasad*[,†]

Institute for Lasers, Photonics and Biophotonics, SUNY at Buffalo, Buffalo, New York 14226, and Department of Chemistry, University of Southern California, Los Angeles, California 90089

ABSTRACT We report a formulation of near-infrared (near-IR) phosphorescent polymeric nanomicelles and their use for in vivo high-contrast optical imaging, targeting, and detection of tumors in small animals. Near-IR phosphorescent molecules of Pt(II)−tetraphenyltetranaphthoporphyrin (Pt(TPNP)) were found to maintain their near-IR phosphorescence properties when encapsulated into phospholipid nanomicelles. The prepared phosphorescent micelles are of ∼100 nm size and are highly stable in aqueous suspensions. A large spectral separation between the Pt(TPNP) absorption, with a peak at ∼700 nm, and its phosphorescence emission, with a peak at ∼900 nm, allows a dramatic decrease in the level of background autofluorescence and scattered excitation light in the near-IR spectral range, where the signal from the phosphorescent probe is observed. In vivo animal imaging with subcutaneously xenografted tumor-bearing mice has resulted in high contrast optical images, indicating highly specific accumulation of the phosphorescent micelles into tumors. Using optical imaging with near-IR phosphorescent nanomicelles, detection of smaller, visually undetectable tumors has also been demonstrated.

KEYWORDS: metalloporphyrins • room-temperature phosphorescence • in vivo optical imaging • polymeric nanomicelles • tumor detection

INTRODUCTION

In the arena of bioimaging, optical imaging possesses a unique position, providing the highest sensitivity and spatial resolution. Optical imaging with fluorescent probes is the only technique which provides cellular or molecular level information with almost single-molecule sensitivity. Therefore, it is being widely used for tracking and reporting functional information on molecules, proteins, and cells/tissues in vitro and in vivo, with a wide range of applications including early diagnosis of cancer and other diseases, study of pharmacokinetics and pharmacodynamics of biomolecules in vivo, and gene expression in light-producing transgenic animals (1, 2). However, in vivo applications of optical bioimaging are severely limited, owing to the poor tissue penetration of visible light. Therefore, in recent years there has been a surge in the development of new generation of optical probes, which absorb and emit light in the near-infrared (near-IR) range (∼700−1000 nm). This spectral region is considered as the "optical transmission window" of biological tissues, where there is less absorption and scattering of the excitation and emitted light as well as reduced autofluorescence, thus allowing penetration of light for deep-tissue imaging with higher contrast (2−4). The recent rise in nanotechnology has further bolstered the prospects of in vivo optical imaging through the development of a variety of near-IR-luminescent nanoformulations, which include quantum dots (5), upconverting nanophosphors (6), and luminophore-containing nanoparticulate carriers such as liposomes (7), polymersomes (8), ceramic (9−11) or polymeric (12) nanoparticles, etc.

Despite a large amount of efforts currently being directed to fight cancer, it continues to be one of the principal diseases, which leads to a large number of fatalities in the world. This is primarily because using currently available techniques the clinical diagnosis of cancer is possible only at extremely advanced phases, when the tumor has extensively metastasized over the body and is thus beyond surgical or chemoradiative intervention. As per the statistical NIH database on pancreatic cancer, currently available on the NIH website, 53% of pancreatic cancer patients have been diagnosed after the cancer has already metastasized (distant stage). Therefore, there is an urgency to the development of novel imaging probes which will diagnose the disease at an earlier, pre-metastatic phase, thus significantly reversing the poor prognostic scenario associated with this disease. Near-IR-luminescent nanoparticles are fast emerging as extremely promising candidates in this direction, as a new generation of optical probes for in vivo imaging. Nanoparticulate optical probes doped with organic near-IR fluorescent molecules demonstrate a number of advantages over molecular near-IR fluorescent probes. First, the nanoparticle formulations provide an option for multimodal imaging by co-doping with imaging agents of other modality,

* To whom correspondence should be addressed. E-mail: pnprasad@buffalo.edu.

Received for review February 28, 2009 and accepted June 2, 2009

[†] SUNY at Buffalo.

[‡] University of Southern California.

DOI: 10.1021/am9001293

Published on Web 06/22/2009

such as MRI (12, 13) and PET/SPECT (14, 15) imaging, thus allowing us to obtain complementary anatomical and physiological information. Next, the surfaces of nanoparticles can be easily modified with (a) inert and biocompatible polymers such as poly(ethylene glycol) (PEG), which endow them with the ability to evade capture and degradation by the reticuloendothelial system (RES) (16, 17), as well as (b) biorecognition molecules to target specific tissues in vivo ("active targeting") (18−21). Finally, upon systemic administration, nanoparticles have an inherent property to be preferentially taken up by the malignant tissues ("passive targeting") by virtue of the "enhanced permeability and retention" (EPR) effect (22, 23), which is the property of such tissues to engulf and retain circulating macromolecules and particles owing to their "leaky" vasculature and poor lymphatic drainage.

Polymeric nanomicelles (PNMs) made up of biocompatible hydrophobic−hydrophilic copolymers (e.g. poloxamers, poloxamines, pluronics, etc.), encapsulating a variety of diagnostic and therapeutic agents, are being increasingly investigated preclinically as safe and efficient drug delivery systems (24). The biocompatible composition of the PNMs, as well as their small size and tunable surface properties, enable them to avoid capture/degradation by RES, thus allowing their unimpeded, prolonged systemic circulation. Drugs encapsulated within PNMs are reported to exhibit higher passive accumulation in tumors compared to free drugs with reduced distribution in other tissues. Recently, PNMs based upon diacyllipid−poly(ethylene glycol) composite molecules have attracted significant attention in drug delivery due to their many unique characteristics. These micelles are stable at extremely low concentrations and demonstrate an increased EPR-mediated passive tumor accumulation (22). In addition, these micelles can be actively targeted to tumor and other desired sites via conjugation with targeting ligands (25, 26).

In this paper, we report the use of polymeric nanomicelles encapsulating near-IR phosphorescent dye (Pt(II)−tetraphenyltetranaphthoporphyrin, Pt(TPNP)) as efficient probes for the high-contrast optical imaging and diagnosis of tumors in small animals. Such phosphorescent molecules as heavy-metal−ligand complexes have been extensively used in the development of organic light emitting devices (OLED) (27−35). In comparison with organic fluorescent dyes, they possess interesting photophysical properties, which make them attractive candidates as probes for autofluorescence-free optical bioimaging. The crucial advantage of the near-IR phosphorescent optical probes over conventional near-IR-fluorescent probes is a large spectral separation between absorption and phosphorescence emission, which ensures a dramatic decrease in the level of background autofluorescence and scattered excitation light in the spectral range where the signal from the phosphorescent probe is observed. In addition, the phosphorescence lifetime for these molecules is essentially different from the characteristic fluorescence lifetime, allowing an opportunity to exploit this highly characteristic feature for time-resolved photoluminescence (PL) imaging (36−40). Time-gated detection can dramatically increase the contrast in imaging, allowing reconstruction of the phosphorescence intensity and lifetime images in scattering (or autofluorescent) volumes (39, 40). A few reports have been recently published on the use of phosphorescent molecules emitting in the visible range for optical imaging in vitro (36−38, 41−45), as well as biolabeling (44) and flow cytometry (45). Formulations of polymeric nanoparticles encapsulating molecules, which phosphoresce in the visible range, have been also reported. However, they are phosphorescent at room temperature only if the atmospheric oxygen is removed (46), if a special polymeric matrix impermeable to oxygen is used (47−49), or, additionally, if the nanoparticle matrix consists of halogen-containing copolymers (49), which are potentially harmful for in vivo applications. On the other hand, in vivo imaging with phosphorescent probes has been known for a long time. Wilson and co-authors first proposed the use of phosphorescent metalloporphyrins as oxygen-sensitive probes for imaging hypoxic tissues in vitro and in vivo (50, 51). Wilson, Vinogradov, and co-authors have further developed their approach, allowing use of phosphorescent probes as oxygen sensors and imaging probes for in vitro and in vivo applications involving imaging of the hypoxic cells and tissues (52). However, these applications were not aimed at the specific targeting of tumors with phosphorescent imaging probes, as tumor sites were not the only sites that were shown to be hypoxic. Here we report the application of a promising and efficient formulation of near-IR phosphorescent polymeric nanomicelles for high-contrast optical imaging in vivo, allowing targeting and detection of tumors in live animals.

EXPERIMENTAL SECTION

Pt(II)−tetraphenyltetranaphthoporphyrin [Pt(TPNP)] was prepared by literature procedures (35, 53). The encapsulation of the Pt(TPNP) into the DSPE-PEG/PC phospholipid micelles was carried out as reported earlier (54, 55) and shown in Figure 1 with several modifications. Typically, 100 μL of phosphorescent dye stock solution in toluene (0.12 mg/mL) was evaporated and dried under vacuum. The obtained solid mass was then resuspended in 1 mL of chloroform with 5.5×10^{-6} mol of phospholipids containing 20% of 1,2-distearoyl-*sn*-glycero-3-phosphoethanolamine-*N*-[methoxy(polyethylene glycol)-2000] (DSPE-mPEG-2000), 20% of 1,2-distearoyl-*sn*-glycero-3-phosphoethanolamine-*N*-[amino(polyethylene glycol)-2000] (DSPE-PEG-2000 NH_2), and 60% of 1,2-distearoylglycero-3-phosphocholine (DSPC), all from Avanti Polar Lipids, Inc., Alabaster, AL. The solution was sonicated for 1 min and the chloroform completely evaporated under vacuum in a rotary evaporator, following which the residue was gently heated at 80 °C and 2 mL of water was added to obtain an optically clear suspension containing DSPE-PEG/PC micelles. Dye/micelle formulation was purified by ultracentrifugation at 500 000 *g* for 2 h. The supernatant was discarded, and the pellet containing phosphorescent dye−micelles was resuspended in water. Different concentrations of the dye-loaded nanomicelles were prepared in the same way as described above by varying the polymer to dye ratio. All the formulations of the phosphorescent dye with approximate concentrations of 2.5, 12.5, and 25 μM were stable in deionized water or phosphate buffered saline (PBS), with no observable aggregation, dissociation, or bleaching for at least 1 month of storage. The samples were stored at 4 °C for further use.

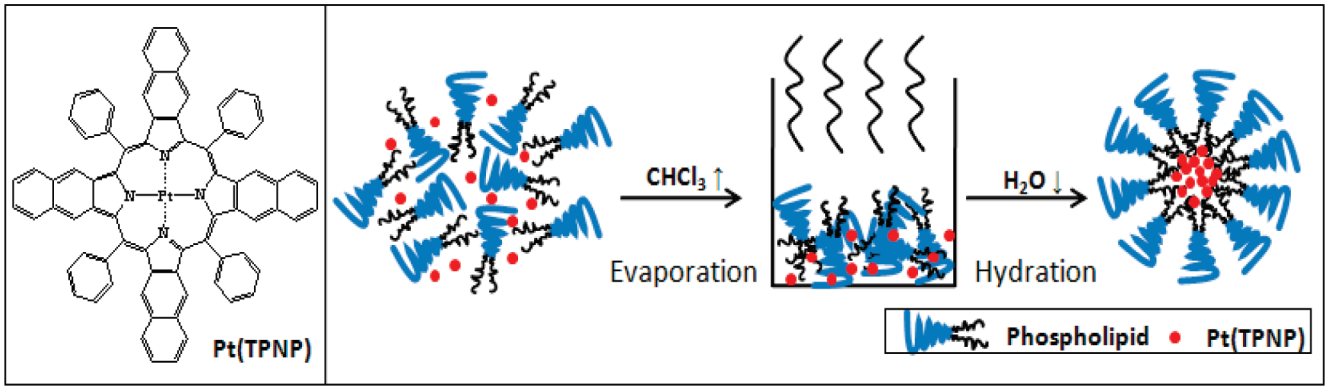

FIGURE 1. Structure of Pt(TPNP) and a scheme showing the procedure used to prepare polymeric nanomicelles by encapsulating the Pt(TPNP) within a PEG-modified phospholipid micelle.

Table 1. Average Hydrodynamic Size of the Polymeric Nanoparticle Formulation Containing Different Concentrations of Pt(TPNP)

	polymer/Pt(TPNP) (w/w)		
	1/0.006	1/0.003	1/0.0006
concn of Pt(TPNP) (μM)	25	12.5	2.5
hydrodynamic diam (nm)	172.6 ± 1.1	153.9 ± 1.5	132.8 ± 1.8
polydispersity	0.212	0.118	0.209

Absorption spectra were acquired using a Shimadzu 3600 spectrophotometer, and a SPEX 270M spectrometer (Jobin Yvon), equipped with an InGaAs TE-cooled photodiode (Electro-Optical Systems, Inc.), was used to record emission spectra. A laser diode emitting at 630 nm was used as an excitation source. The sample in a quartz cuvette was placed directly in front of the entrance slit of the spectrometer, and the emission signal was collected at 90° relative to the excitation light. A Hamamatsu IR-PMT, attached to the second output port of the SPEX 270M spectrometer, was used to record emission decays on the Infinium oscilloscope (Hewlett-Packard) coupled to the output of the PMT. A third harmonic (355 nm) from a nanosecond pulsed Nd:YAG laser (Lotis TII, Belarus), operating at 20 Hz, was used as the excitation source.

The xenografted mouse models were generated by subcutaneously injecting Panc-1 cells at a concentration of (2−3) × 10^6 cells/mouse in the scapular region of 5−6-week-old female athymic nude mice (Hsd:Athymic Nude-*Foxn1*^{nu}) using a 1 mL Monoject tuberculin syringe. Tumor growth was monitored every 24−48 h until a tumor size of approximately 5 mm in diameter was observed. The tumored mice was injected with the 200 μL of the nanoparticle formulation (30 μg/mL) in water with 5% glucose and imaged at different time points starting at 2 h to 96 h post-injection to study the biodistribution of the nanoparticle formulation in tumor and other major organs.

RESULTS AND DISCUSSION

Dynamic light scattering (DLS) studies were carried out to determine the hydrodynamic diameter of the nanomicelles. The size of the polymeric micelles varies with the loading of the Pt(TPNP) with the polymer showing the dependence of size on the polymer to dye ratio. Depending upon the polymer to Pt(TPNP) ratio, the hydrodynamic size of the polymeric nanomicelles varied between ~130 and 170 nm (Table 1).

The dimension and morphology of the polymeric nanoparticle formulation were further characterized by transmission electron microscopy (TEM) using a JEOL Model JEM-100CX microscope operating at an acceleration voltage of 80 kV. To visualize the phospholipid layer, the samples were negatively stained using 1% PTA (phosphotungstic acid) at pH 7. With this technique, the stained phospholipid micelles doped with Pt(TPNP) can be visualized as irregular shaped light disks with average diameter at around 100 nm that stand out against the stained dark background (Figure 2).

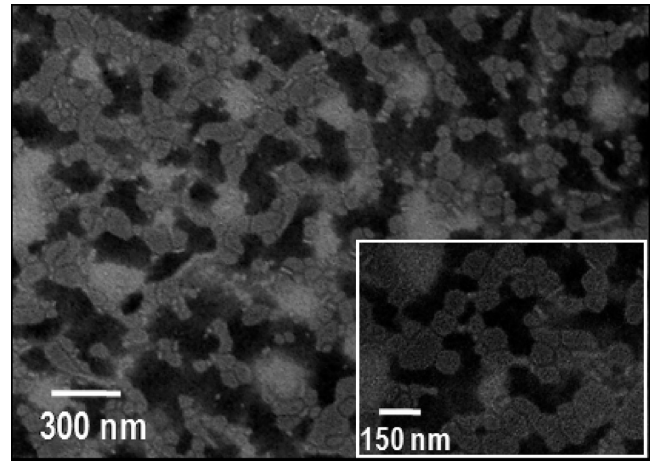

FIGURE 2. Representative TEM images of the Pt(TPNP)/DSPE-PEG/PC nanomicelles.

Photophysical characterization of Pt(TPNP) in $CHCl_3$ and DSPE-PEG/PC nanomicelles was performed using absorption and photoluminescence spectroscopy. Results of the photophysical characterization of Pt(TPNP) are shown in Figure 3. Absorption and emission spectra of Pt(TPNP) in organic solvent are similar to those reported for Pt(II)−tetraphenyltetrabenzoporphyrin, Pt(TPBP) (30). Pt(TPNP) has the first absorption maximum at 691 nm and the emission peak at 903 nm, against 611 and 765 nm in the case of Pt(TPBP). This bathochromic shift originates from the extension of the π system by replacing the benzannulated phenyl group of Pt(TPBP) with a benzannulated naphthyl group in Pt(TPNP). The emission from the Pt(TPNP) is phosphorescence facilitated by a heavy-metal atom (Pt) which increases the rate of the intersystem crossing between singlet and triplet states of the metalloporphyrins, thereby enhancing the rate of radiative decay from the triplet state (30, 56, 57). Absorption and emission of the Pt(TPNP) in DSPE-PEG/PC nanomicelles are close to those of Pt(TPNP) in $CHCl_3$, except for strong

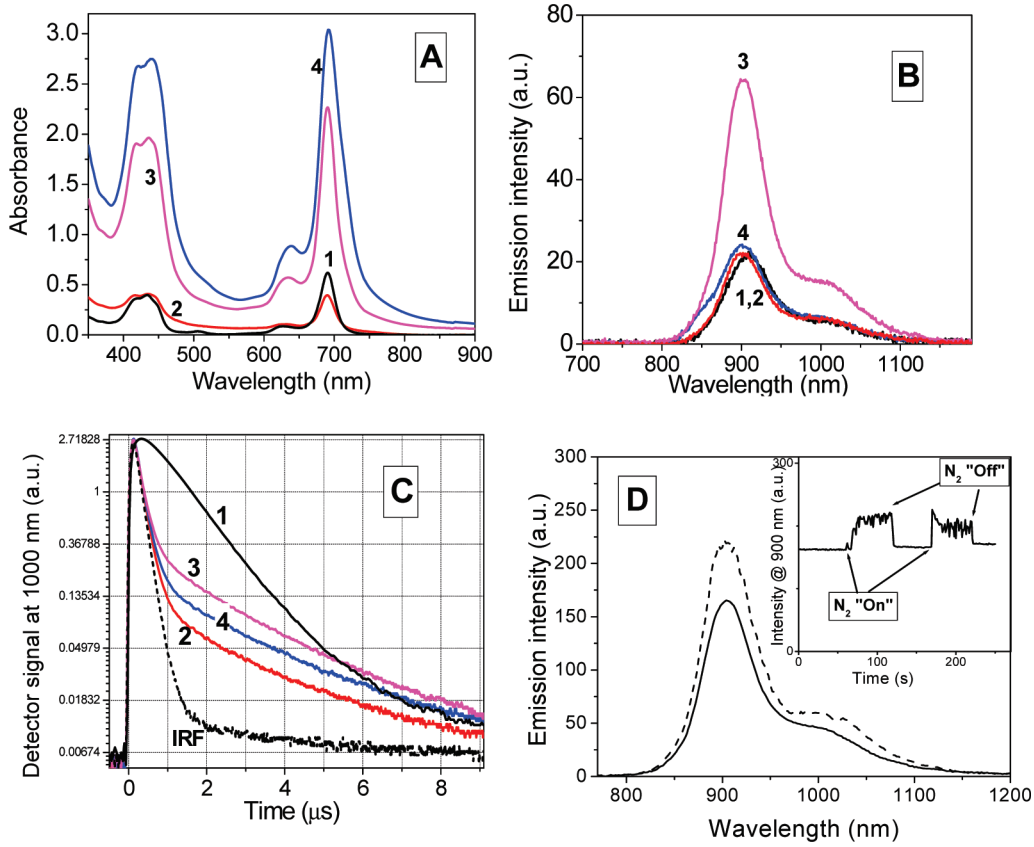

FIGURE 3. Absorption (A) and emission spectra (B) and emission decays (C) from Pt(TPNP) in $CHCl_3$ (1) and DSPE-PEG/PC nanomicelles (2−4) at room temperature. Concentrations of Pt(TPNP): 2.5 μM (1, 2), 12.5 μM (3), 25 μM (4). (D) Pt(TPNP)/DSPE-PEG/PC phosphorescence spectra in the presence of oxygen (solid line) and under nitrogen purging (dashed line). The inset shows changes in the phosphorescence intensity at 900 nm with N_2 bubbling turned on and off.

quenching of phosphorescence from Pt(TPNP) in DSPE-PEG/PC with an increase in concentration (Figure 3B). This is apparently caused by the aggregation of the metalloporphyrin molecules within micelles which dominates at the high ratios of Pt(TPNP) to DSPE-PEG/PC and leads to triplet−triplet annihilation (58). Manifestation of this aggregation can be also seen in absorption spectra (59−61), where, due to the lower extinction of aggregates in comparison with that of monomers, a 2-fold increase in concentration results in only a ~30% increase in absorption intensity (Figure 3A, curves 3 and 4). However at lower ratios of Pt(TPNP) to DSPE-PEG/PC, phosphorescence of the metalloporphyrin in polymeric nanomicelles is at least as efficient as in organic solvent. As can be seen in Figure 3C, phosphorescence decays of Pt(TPNP) in $CHCl_3$ as well as in DSPE-PEG/PC cannot be fitted to a single exponential but can be characterized by the average decay time: 3.3−3.9 μs for Pt(TPNP) in DSPE-PEG/PC and ~1.3 μs for Pt(TPNP) in $CHCl_3$. It should be noted that room-temperature phosphorescence is highly sensitive to the environment. The longer phosphorescence lifetime of Pt(TPNP) when it is encapsulated within polymeric micelles, over that when it is dissolved in an organic solution, can be explained, in particular, by a hindered access of quenchers: i.e., oxygen molecules. The phosphorescence quantum yield (φ_{ph}) was measured, using a methanol solution of indocyanine green dye (fluorescence quantum yield of 0.12 (62)) as a reference (see the Supporting information), and was found to be 0.01. Taking into account that φ_{ph} of Pt(TPNP) in argon-degassed toluene was reported to be 0.22 (35), one can suggest that the phosphorescence of Pt(TPNP) in micelles is strongly quenched by oxygen. However, we have found that purging of the Pt(TPNP)/DSPE-PEG/PC dispersion with nitrogen results in only a ~25−30% increase in the phosphorescence intensity of the Pt(TPNP) (Figure 3D). This can be explained by the encapsulation of the Pt(TPNP) within polymeric micelles, which significantly hinders access by oxygen molecules, similarly to that reported for dendrimers with Pd/Pt porphyrin cores (52, 63). Thus, factors other than the presence of oxygen are possibly playing major roles in the quenching of Pt(TPNP) phosphorescence within micelles. Probably this quenching is a result of intramolecular interactions (aggregation of the metalloporphyrin molecules) taking place within micelles, as indicated in Figure 3A,B.

We believe that, even if the phosphorescence quantum yield of the investigated Pt(TPNP)/DSPE-PEG/PC formulation is found to be not high, it will still be useful in optical imaging applications, considering the high molar extinction coefficient of the absorption band with peak at 691 nm, the spectral range where phosphorescence is observed and large spectral separation of the excitation and emission wavelengths. In addition, excitation/emission of the Pt(TPNP) is red-shifted in comparison with that of previously reported near-IR phosphorescent probes, thus allowing deeper tissue

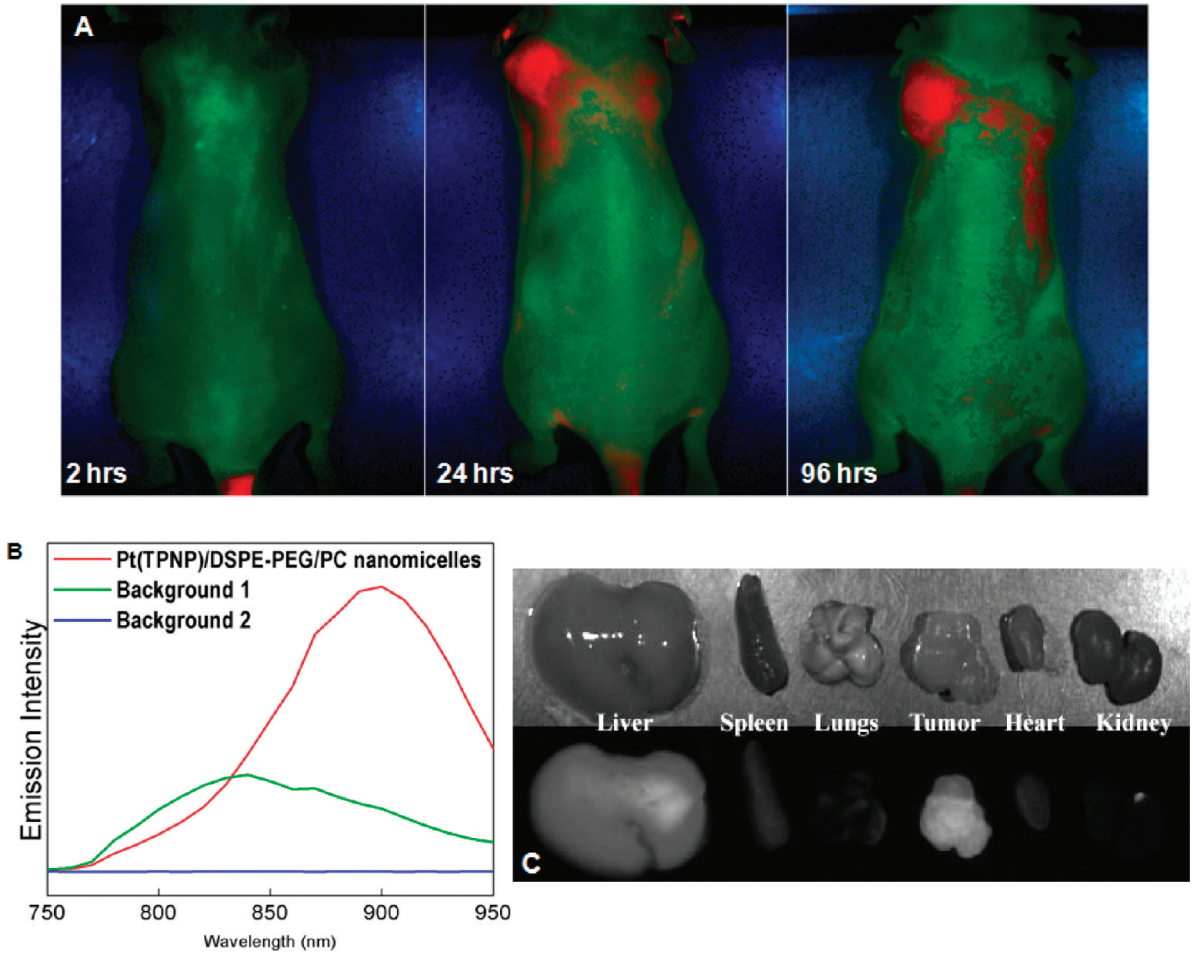

FIGURE 4. (A) PL images of the tumored nude mouse at various time points (2, 24, 96 h) postinjection with the nanomicelles. (B) Spectral profiles used to unmix images shown in (A). (C) Bright field and PL images of the major organs resected from mouse 96 h postinjection.

penetration and less background signal (scattering and autofluorescence) during imaging. While the absence of oxygen-mediated strong phosphorescence quenching of the Pt(TPNP)/DSPE-PEG/PC nanomicelles impedes their use for imaging hypoxic tissues in vivo, it favors their use as nanoparticulate probes for optical imaging in vivo. All these results, along with excellent colloidal stablility of the Pt-(TPNP)/DSPE-PEG/PC nanomicelles, prompted us to investigate their applicability in near-IR phosphorescence optical imaging in vivo. Since the stability of nanomicelles is of importance for optical imaging, we have also tested a possible leakage of the entrapped Pt(TPNP) from DSPE-PEG/PC micelles. The release kinetics study has shown that the release of the Pt(TPNP) from micelles was insignificant, when Pt(TPNP)/DSPE-PEG/PC nanomicelles were incubated with 1% of the Tween-80 surfactant at 37 °C (see the Supporting Information).

We have tested the cytotoxicity of the Pt(TPNP)/DSPE-PEG/PC nanomicelles by performing a cell viability (MTS) assay (64), which was carried out with pancreatic cancer cell line Panc-1 (ATCC, CRL-1469), showing slight, dose-dependent toxicity of the nanomicelles over a period of 24 h (see the Supporting Information). The nanoparticle formulation showed also no overt short-term toxicity in the injected mice after 96 h postinjection.

To verify the applicability the Pt(TPNP)/DSPE-PEG/PC nanomicelles for in vivo optical imaging and their possible tumor targeting ability, we injected them intravenously (tail vein) in nude mice bearing subcutaneous pancreatic tumor xenografts. In vivo PL imaging was accomplished using the Maestro GNIR FLEX fluorescence imaging system (CRi) (for details, see the Supporting Information). The phosphorescent dye formulation was excited using a "deep red" excitation filter (CRi), transmitting light from the source (Xe lamp) in the range of 650−700 nm. A near-IR emission filter (800 LP) in front of the imaging CCD camera was used to cut off the excitation light. Figure 4 presents results of the in vivo imaging. The whole-body images of the tumored nude mouse injected with nanomicelles were taken at various time points postinjection and spectrally unmixed using the Maestro imaging software. The high-contrast images clearly demonstrate the feasibility to spectrally distinguish and image the phosphorescence from Pt(TPNP) (shown as red). Figure 4B shows spectral profiles used to unmix the images shown in Figure 4A; spectral signatures from backgrounds 1 and 2 were sampled from the imaging stage and preinjected mouse, respectively; an intense near-IR emission spectrum peak at around 900 nm was acquired from the vial with the Pt(TPNP)/DSPE-PEG/PC nanomicelles. As can be clearly seen in Figure 4A, there is an intense phosphores-

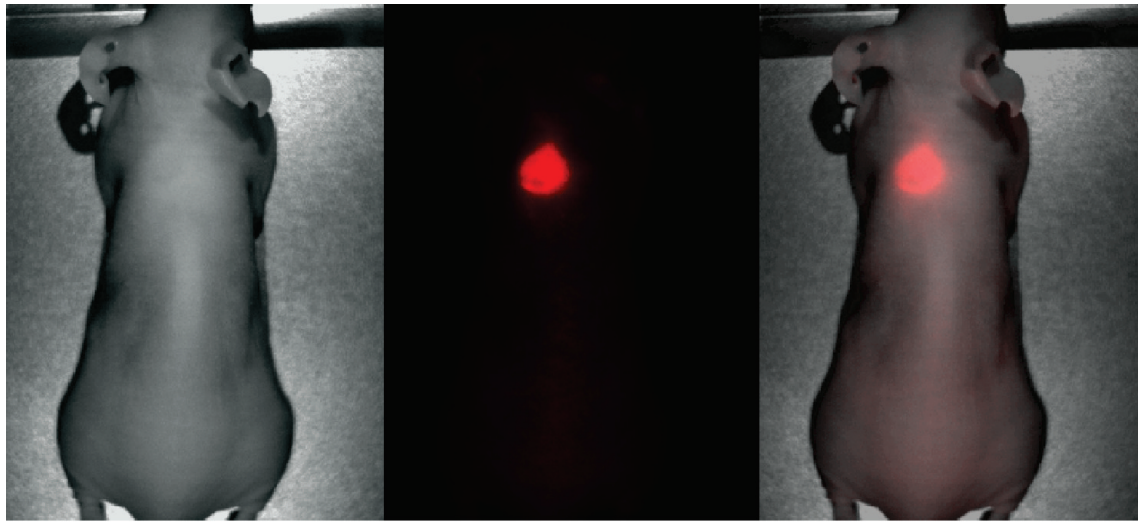

A B C

FIGURE 5. Bright field (A), phosphorescence (B), and combined (C) images of the nude mouse xenografted with a subcutaneous Panc 1 tumor in its early phase of growth. (1 week after tumor cells injection). Images were taken 24 h after IV injection of the Pt(TPNP)/DSPE-PEG/PC nanomicelles.

cence from the tumor at 24 and 96 h postinjection, while the 2 h postinjection image shows only a bright signal at the injection site (tail). Some emission from nanomicelles still can be seen in the lower abdominal region and in the liver, when the mouse was imaged from the dorsal side (see the Supporting Information). It is quite evident that with a longer time period (24−96 h postinjection) the accumulation of the Pt(TPNP)/DSPE-PEG/PC nanomicelles in the tumor takes place, although a considerable amount of the phosphorescence can be observed in the liver as well. This can be attributed to the prolonged circulation time of the Pt(TPNP)/DSPE-PEG/PC nanomicelles, thus facilitating their passive tumor uptake via the EPR effect (22, 23) However, a release of the Pt(TPNP) from nanomicelles in vivo can also contribute to tumor targeting (65), thus exploiting the possible specificity of the porphyrin-based molecules toward cancer cells (66). Thus, the tumor-targeting ability of the Pt(TPNP)/DSPE-PEG/PC nanomicellar formulation can be caused by both the EPR effect for the polymeric micelles and possible inherent tumor avidity of Pt(TPNP), resulting in efficient labeling of the xenografted tumors in vivo. Further work needs to be done to clarify the mechanism of tumor targeting for the Pt(TPNP)/DSPE-PEG/PC nanomicelles.

Figure 4C visualizes a biodistribution of the nanomicelles in major organs. To carry out the studies, organs were resected after 96 h and imaged immediately, keeping the same parameters as for whole body in vivo imaging. The biodistribution results confirmed the accumulation of the polymeric nanomicelles mainly in the tumor and liver. It is interesting to note that phosphorescence from the liver bleeds through the back of the mouse (Figure 4A, 24 and 96 h), illustrating better tissue penetration for the near-IR light. The amount of the phosphorescence observed in other organs was insignificant.

Nanoparticles of different types are known to be efficiently captured by the liver (67), but the relative amount of phosphorescence from the Pt(TPNP)/DSPE-PEG/PC nanomicelles which is seen in the tumor is quite remarkable. The phosphorescence intensity from the tumor looks even higher than that from the liver, thus implying a high efficiency of passive tumor targeting in our system, which is not observed in previous reports of passive tumor targeting employing other formulations of the DSPE-PEG nanomicelles and other PEG-grafted formulations (68). Recently, Park et al. (12) reported preparation and in vivo application of the PEG-phospholipid nanomicelles, co-doped with near-IR emitting quantum dots, magnetic nanoparticles, and anticancer drug for bimodal (optical and MRI) imaging and drug delivery, and showed a moderate degree of tumor accumulation, which was significantly lower as compared to the liver accumulation. We believe that tumor specificity of the Pt(TPNP)/DSPE-PEG/PC nanomicelles can be even further improved by modifying the composition to optimize their size distribution and/or surface properties, as well as incorporating biorecognition molecules on their surface for target specific delivery (19−21, 69).

Following this, we have investigated whether it is possible to diagnose even smaller, visually undetectable subcutaneous tumors in mice using this phosphorescent nanomicellar formulation. With this purpose, we have intravenously injected the Pt(TPNP)/DSPE-PEG/PC nanomicelles in nude mice only 1 week following cancer cell inoculation. Visually undetectable small tumors demonstrated intense phosphorescence 24 h post injection of phosphorescent nanomicelles (Figure 5), thus demonstrating the ability of Pt(TPNP)/DSPE-PEG/PC formulation to detect tumors at very early stages of their development. In order to verify whether a local damage of the vasculature as a result of the injection of cancer cells is not a factor promoting accumulation of the phosphorescent micelles, a control experiment was performed. Here, non-tumored mouse was subcutaneously injected with saline, and subsequently injected in tail vein with Pt(TPNP)/

DSPE-PEG/PC nanomicelles and imaged 24 h later. No localization of the Pt(TPNP)/DSPE-PEG/PC nanomicelles at the injected site was observed, thus suggesting the specificity of the formulation toward the tumor tissue (see the Supporting Information).

CONCLUSIONS

In conclusion, these nanosized probes for detection of cancer in a noninvasive manner can have significant clinical implications on cancer diagnostics and therapeutics. On the basis of all the preliminary results, it can be concluded that the phosphorescent polymeric nanomicellar formulation provides a powerful tool for in vivo optical imaging and carries great promise as an efficient optical imaging probe aimed at the detection and imaging of tumors. Detailed studies with the micellar formulation are underway, including histopathological studies and studies using more advanced tumor models, including mice bearing orthotopically implanted spontaneously metastasizing pancreatic tumors.

Acknowledgment. This work was supported by grants from the National Institutes of Health (Nos. R01CA119397 and RO1CA104492) and the John R. Oishei Foundation. We also thank Lisa A. Vathy for her technical support.

Supporting Information Available: Text and figures giving details of transmission electron microscopy, the in vivo optical imaging setup, the MTS assay, release kinetics studies, PL quantum yield measurements, and PL images. This material is available free of charge via the Internet at http://pubs.acs.org.

REFERENCES AND NOTES

(1) Michaelis, J.; Hettich, C.; Mlynek, J.; Sandoghdar, V. *Nat. Med.* **2000**, *405*, 586.
(2) Prasad, P. N. *Introduction to Biophotonics*; Wiley-Interscience: New York, 2004.
(3) Weissleder, R. *Nat. Biotechnol.* **2001**, *19*, 316.
(4) Sevick-Muraca, E. M.; Houston, J. P.; Gurfinkel, M. *Curr. Opin. Chem. Biol.* **2002**, *6*, 642.
(5) Kim, S.; Lim, Y. T.; Soltesz, E. G.; De Grand, A. M.; Lee, J.; Nakayama, A.; Parker, J. A.; Mihaljevic, T.; Laurence, R. G.; Dor, D. M.; Cohn, L. H.; Bawendi, M. G.; Frangioni, J. V. *Nat. Biotechnol.* **2004**, *22*, 93.
(6) Nyk, M.; Kumar, R.; Ohulchanskyy, T. Y.; Bergey, E. J.; Prasad, P. N. *Nano Lett.* **2008**, *8*, 3834.
(7) Deissler, V.; Ruger, R.; Frank, W.; Fahr, A.; Kaiser, W. A.; Hilger, I. *Small* **2008**, *4*, 1240.
(8) Ghoroghchian, P. P.; Frail, P. R.; Susumu, K.; Blessington, D.; Brannan, A. K.; Bates, F. S.; Chance, B.; Hammer, D. A.; Therien, M. J. *Proc. Natl. Acad. Sci. U.S.A.* **2005**, *102*, 2922.
(9) Altinoglu, E. I.; Russin, T. J.; Kaiser, J. M.; Barth, B. M.; Eklund, P. C.; Kester, M.; Adair, J. H. *ACS Nano* **2008**, *2*, 2075.
(10) Josephson, L.; Kircher, M. F.; Mahmood, U.; Tang, Y.; Weissleder, R. *Bioconjugate Chem.* **2002**, *13*, 554.
(11) He, X.; Nie, H.; Wang, K.; Tan, W.; Wu, X.; Zhang, P. *Anal. Chem.* **2008**, *80*, 9597.
(12) Park, J. H.; von Maltzahn, G.; Ruoslahti, E.; Bhatia, S. N.; Sailor, M. J. *Angew. Chem., Int. Ed.* **2008**, *47*, 7284.
(13) Haacke, E. M.; Brown, R. W.; Thompson, M. L.; Venkatesan, R. *Magnetic Resonance Imaging: Physical Principles and Sequence Design*; Wiley: New York, 1999.
(14) Nahrendorf, M.; Zhang, H. W.; Hembrador, S.; Panizzi, P.; Sosnovik, D. E.; Aikawa, E.; Libby, P.; Swirski, F. K.; Weissleder, R. *Circulation* **2008**, *117*, 379.
(15) Shokeen, M.; Fettig, N. M.; Rossin, R. Q. J. *Nucl. Med. Mol. Imaging* **2008**, *52*, 267.
(16) Jain, T. K.; Roy, I.; De, T. K.; Maitra, A. *J. Am. Chem. Soc.* **1998**, *120*, 11092.
(17) Esmaeili, F.; Ghahremani, M. H.; Esmaeili, B.; Khoshayand, M. R.; Atyabi, F.; Dinarvand, R. *Int. J. Pharm.* **2008**, *349*, 249.
(18) Esmaeili, F.; Ghahremani, M. H.; Ostad, S. N.; Atyabi, F.; Seyedabadi, M.; Malekshahi, M. R.; Amini, M.; Dinarvand, R. *J. Drug Targeting* **2008**, *16*, 415.
(19) Leuschner, C.; Kumar, C. S. S. R.; Hansel, W.; Soboyejo, W.; Zhou, J. K.; Hormes, J. *Breast Cancer Res. and Treatment* **2006**, *99*, 163.
(20) Byrne, J. D.; Betancourt, T.; Brannon-Peppas, L. *Adv. Drug Delivery Rev.* **2008**, *60*, 1615.
(21) Kirpotin, D. B.; Drummond, D. C.; Shao, Y.; Shalaby, M. R.; Hong, K. L.; Nielsen, U. B.; Marks, J. D.; Benz, C. C.; Park, J. W. *Cancer Res.* **2006**, *66*, 6732.
(22) Lukyanov, A. N.; Gao, Z. G.; Mazzola, L.; Torchilin, V. P. *Pharm. Res.* **2002**, *19*, 1424.
(23) Maeda, H.; Wu, J.; Sawa, T.; Matsumura, Y.; Hori, K. *J. Controlled Release* **2000**, *65*, 271.
(24) Torchilin, V. P. *Pharm. Res.* **2007**, *24*, 1.
(25) Roby, A.; Erdogan, S.; Torchilin, V. P. *Cancer Biol. Therapy* **2007**, *6*, 1136.
(26) Skidan, I.; Dholakia, P.; Torchilin, V. *J. Drug Targeting* **2008**, *16*, 486.
(27) Baldo, M. A.; O'Brien, D. F.; You, Y.; Shoustikov, A.; Sibley, S.; Thompson, M. E.; Forrest, S. R. *Nature* **1998**, *395*, 151.
(28) Brooks, J.; Babayan, Y.; Lamansky, S.; Djurovich, P. I.; Tsyba, I.; Bau, R.; Thompson, M. E. *Inorg. Chem.* **2002**, *41*, 3055.
(29) Chou, P. T.; Chi, Y. *Chem. Eur. J.* **2007**, *13*, 380.
(30) Borek, C.; Hanson, K.; Djurovich, P. I.; Thompson, M. E.; Aznavour, K.; Bau, R.; Sun, Y. R.; Forrest, S. R.; Brooks, J.; Michalski, L.; Brown, J. *Angew. Chem., Int. Ed.* **2007**, *46*, 1109.
(31) Sun, Y.; Borek, C.; Hanson, K.; Djurovich, P. I.; Thompson, M. E.; Brooks, J.; Brown, J. J.; Forrest, S. R. *Appl. Phys. Lett.* **2007**, *90*, 263503.
(32) Sun, Y. R.; Giebink, N. C.; Kanno, H.; Ma, B. W.; Thompson, M. E.; Forrest, S. R. *Nature* **2006**, *440*, 908.
(33) Baldo, M. A.; Lamansky, S.; Burrows, P. E.; Thompson, M. E.; Forrest, S. R. *Appl. Phys. Lett.* **1999**, *75*, 4.
(34) Yersin, H. *Top. Curr. Chem.* **2004**, *241*, 1 (Transition Metal and Rare Earth Compounds III).
(35) Sommer, J. R.; Farley, R. T.; Graham, K. R.; Yang, Y.; Reynolds, J. R.; Xue, J.; Schanze, K. S. *ACS Appl. Mater. Interfaces* **2009**, *1*, 274.
(36) de Haas, R. R.; van Gijlswijk, R. P. M.; van der Tol, E. B.; Zijlmans, H. J. M. A. A.; BakkerSchut, T.; Bonnet, J.; Verwoerd, N. P.; Tanke, H. J. *J. Histochem. Cytochem.* **1997**, *45*, 1279.
(37) Botchway, S. W.; Charnley, M.; Haycock, J. W.; Parker, A. W.; Rochester, D. L.; Weinstein, J. A.; Williams, J. A. G. *Proc. Natl. Acad. Sci. U.S.A.* **2008**, *105*, 16071.
(38) de Haas, R. R.; van Gijlswijk, R. P. M.; van der Tol, E. B.; Veuskens, J.; van Gijssel, H. E.; Tijdens, R. B.; Bonnet, J.; Verwoerd, N. P.; Tanke, H. J. *J. Histochem. Cytochem.* **1999**, *47*, 183.
(39) Apreleva, S. V.; Wilson, D. E.; Vinogradov, S. A. *Optics Lett.* **2006**, *31*, 1082.
(40) Apreleva, S. V.; Wilson, D. F.; Vinogradov, S. A. *Appl. Optics* **2006**, *45*, 8547.
(41) Yu, M. X.; Zhao, Q.; Shi, L. X.; Li, F. Y.; Zhou, Z. G.; Yang, H.; Yia, T.; Huang, C. H. *Chem. Commun.* **2008**, *18*, 2115.
(42) Amoroso, A. J.; Arthur, R. J.; Coogan, M. P.; Court, J. B.; Fernandez-Moreira, V.; Hayes, A. J.; Lloyd, D.; Millet, C.; Pope, S. J. A. *New J. Chem.* **2008**, *32*, 1097.
(43) Amoroso, A. J.; Coogan, M. P.; Dunne, J. E.; Fernandez-Moreira, V.; Hess, J. B.; Hayes, A. J.; Lloyd, D.; Millet, C.; Pope, S. J. A.; Williams, C. *Chem. Commun.* **2007**, *29*, 3066.
(44) Lo, K. K. W.; Louie, M. W.; Sze, K. S.; Lau, J. S. Y. *Inorg. Chem.* **2008**, *47*, 602.
(45) Lo, K. K. W.; Lee, T. K. M.; Lau, J. S. Y.; Poon, W. L.; Cheng, S. H. *Inorg. Chem.* **2008**, *47*, 200.
(46) Pfister, A.; Zhang, G.; Zareno, J.; Horwitz, A. F.; Fraser, C. L. *ACS Nano* **2008**, *2*, 1252.
(47) Kurner, J. M.; Klimant, I.; Krause, C.; Preu, H.; Kunz, W.; Wolfbeis, O. S. *Bioconjugate Chem.* **2001**, *12*, 883.
(48) Kurner, J. M.; Klimant, I.; Krause, C.; Pringsheim, E.; Wolfbeis, O. S. *Anal. Biochem.* **2001**, *297*, 32.
(49) Song, X.; Huang, L.; Wu, B. *Anal. Chem.* **2008**, *80*, 5501.
(50) Rumsey, W. L.; Vanderkooi, J. M.; Wilson, D. F. *Science* **1988**, *241*, 1649.

(51) Wilson, D. F.; Rumsey, W. L.; Green, T. J.; Vanderkooi, J. M. *J. Biol. Chem.* **1988**, *263*, 2712.
(52) Brinas, R. P.; Troxler, T.; Hochstrasser, R. M.; Vinogradov, S. A. *J. Am. Chem. Soc.* **2005**, *127*, 11851.
(53) Perez, D. M.; Borek, C.; Forrest, S. R.; Thompson, M. E. Submitted for publication in *J. Am. Chem. Soc.*
(54) Cinteza, L. O.; Ohulchanskyy, T. Y.; Sahoo, Y.; Bergey, E. J.; Pandey, R. K.; Prasad, P. N. *Mol. Pharm.* **2006**, *3*, 415.
(55) Zheng, Q.; Ohulchanskyy, T. Y.; Sahoo, Y.; Prasad, P. N. *J. Phys. Chem. C* **2007**, *111*, 16846.
(56) Chandra, A. K.; Turro, N. J.; Lyons, A. L.; Stone, P. *J. Am. Chem. Soc.* **1978**, *100*, 4964.
(57) Papkovsky, D. B. *Sens. Actuators B* **1995**, *29* (1−3), 213–218.
(58) Turro, N. J.; Aikawa, M. *J. Am. Chem. Soc.* **1980**, *102*, 4866.
(59) Pugh, D.; Giles, C. H.; Duff, D. G. *Trans. Faraday Soc.* **1971**, *67*, 563.
(60) Gandini, S. C. M.; Yushmanov, V. E.; Borissevitch, I. E.; Tabak, M. *Langmuir* **1999**, *15*, 6233.
(61) Li, X. Y.; He, X.; Ng, A. C. H.; Wu, C.; Ng, D. K. P. *Macromolecules* **2000**, *33*, 2119.
(62) Philip, R.; Penzkofer, A.; Baumler, W.; Szeimies, R. M.; Abels, C. *J. Photochem. Photobiol. A* **1996**, *96*, 137.
(63) Rozhkov, V.; Wilson, D.; Vinogradov, S. *Macromolecules* **2002**, *35*, 1991.
(64) Cory, A. H.; Owen, T. C.; Barltrop, J. A.; Cory, J. G. *Cancer Commun.* **1991**, *3*, 207.
(65) Chen, H. T.; Kim, S. W.; Li, L.; Wang, S. Y.; Park, K.; Cheng, J. X. *Proc. Natl. Acad. Sci. U.S.A.* **2008**, *105*, 6596.
(66) Song, R.; Kim, Y. S.; Sohn, Y. S. *J. Inorg. Biochem.* **2002**, *89*, 83.
(67) Brigger, I.; Dubernet, C.; Couvreur, P. *Adv. Drug Delivery Rev.* **2002**, *54*, 631.
(68) Torchilin, V. P. *Eur. J. Pharm. Biopharm.* **2009**, *71*, 431.
(69) Torchilin, V. *Expert Opin. Drug Delivery* **2008**, *5*, 1003.

AM9001293